iScience

CellPress
OPEN ACCESS

Article

Near-infrared light photocatalysis enabled by a ruthenium complex-integrated metal–organic framework via two-photon absorption

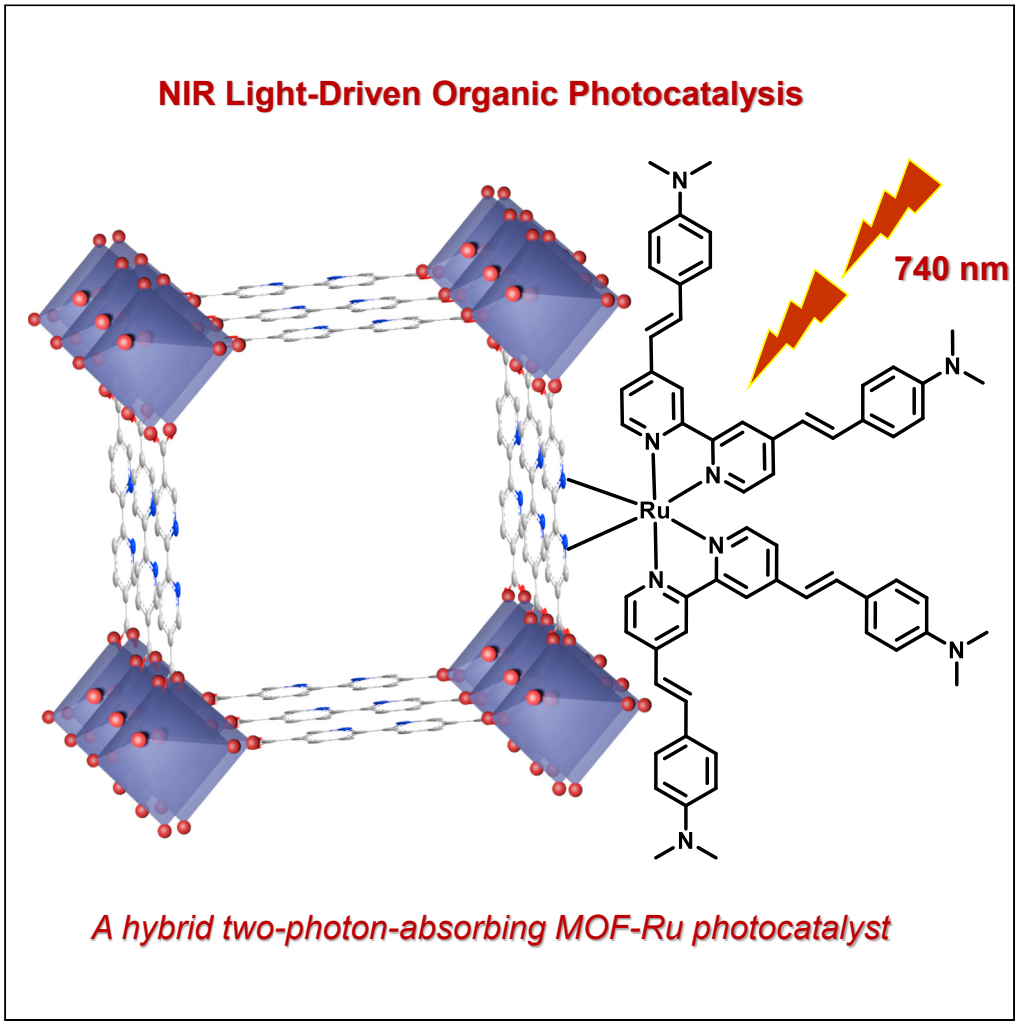

Jian-Hong Tang, Guanqun Han, Guodong Li, Kaili Yan, Yujie Sun

yujie.sun@uc.edu

Highlights

Ru complexes with π-conjugation ligands show two-photon absorption of NIR photons

Hybrid MOF-Ru has NIR light-driven photocatalytic performance with recyclability

A variety of organic reactions were photocatalyzed by MOF-Ru under 740 nm irradiation

Tang et al., iScience *25*, 104064
April 15, 2022
https://doi.org/10.1016/j.isci.2022.104064

iScience

CellPress
OPEN ACCESS

Article

Near-infrared light photocatalysis enabled by a ruthenium complex-integrated metal–organic framework via two-photon absorption

Jian-Hong Tang,[1,2] Guanqun Han,[1,2] Guodong Li,[1] Kaili Yan,[1] and Yujie Sun[1,3,*]

SUMMARY

Photocatalysis under UV/visible light irradiation has emerged as one of the green methodologies for solar energy utilization and organic synthesis. These photocatalytic processes are typically initiated by one-photon-absorbing metal complexes or organic dyes. Nevertheless, the intrinsic restrictions of UV/visible light irradiation, such as shallow penetration in reaction solutions, competing absorption by substrates, and limited coverage of the solar spectrum, call for the development of innovative photocatalysts functioning under longer wavelength irradiation. Herein, we report a ruthenium complex containing a metal-organic framework, MOF-Ru1, which can drive diverse organic reactions under 740 nm light irradiation following the two-photon absorption (TPA) process. Various organic transformations such as energy transfer, reductive, oxidative, and redox neutral reactions were realized using this heterogeneous hybrid photocatalyst. Overall, MOF-Ru1 represents an intriguing TPA photocatalyst active under near-infrared light irradiation, paving a way for the efficient utilization of low-energy light and convenient photocatalyst recycling because of phase separation.

INTRODUCTION

Organic photocatalysis has witnessed a rapid renaissance over the past two decades, thanks to the advancements in photosensitizer development and elegant reaction design (Ciamician, 1912; Prier et al., 2013; Zhang et al., 2019; Nicewicz and MacMillan, 2008; Schultz and Yoon, 2014). Regardless of the light-absorbing species in conventional organic photocatalysis, such as transition metal complexes (Twilton et al., 2017; Dolgopolova et al., 2018; Glaser et al., 2020; Glaser and Wenger, 2020), organic dyes (Twilton et al., 2017), and semiconductors (Li et al., 2020; Caputo et al., 2017; Kisch, 2017), the typical photon source is either UV or visible-light irradiation because these photons are able to provide sufficient energy (50–80 kcal/mol) for desirable organic transformations. Nevertheless, UV/visible-light photocatalysis may be accompanied by several intrinsic limitations such as competing light absorption by organic substrates which restricts reaction scope, as well as shallow light penetration depth that hampers large-scale deployment (Yoon et al., 2010; Buzzetti et al., 2019). Comparatively, infrared (IR) light accounts for more than 50% of the energy in solar irradiation and is also able to circumvent the aforementioned UV/visible-light limitations (Zhou et al., 2020; Günes et al., 2007). However, near-IR light-driven organic photocatalysis has remained largely underexplored because of the low-energy of IR photons.

Unlike UV/visible-light photocatalysis, which only needs to absorb one photon per step to access the excited state of desirable energy (Figure 1A), near-IR photons can only excite molecules to an excited state of lower energy, ca. 35 kcal/mol, inadequate for the majority of useful organic reactions. Therefore, concurrent two (or more) photon absorption in the longer wavelength region (>700 nm) is necessary for near-IR light-driven organic photocatalysis (Zhou et al., 2015; Park et al., 2015; Zheng et al., 2018; Fallon et al., 2020; Majek et al., 2015). In general, there exist two strategies of utilizing low-energy photons to produce high-energy excited states: (i) triplet-triplet annihilation (TTA, Figure 1B) and (ii) direct two-photon absorption (TPA, Figure 1C). Following the TTA mechanism, the sensitizer absorbs low-energy photons to populate their corresponding triplet-excited states which individually activate two annihilators via energy transfer. The resulting two annihilators at triplet-excited state follow a triplet-fusion upconversion step to generate one activated annihilator at the singlet-excited state with higher energy and the other back to the

[1]Department of Chemistry, University of Cincinnati, Cincinnati, OH 45221, USA

[2]These authors contributed equally

[3]Lead contact

*Correspondence: yujie.sun@uc.edu

https://doi.org/10.1016/j.isci.2022.104064

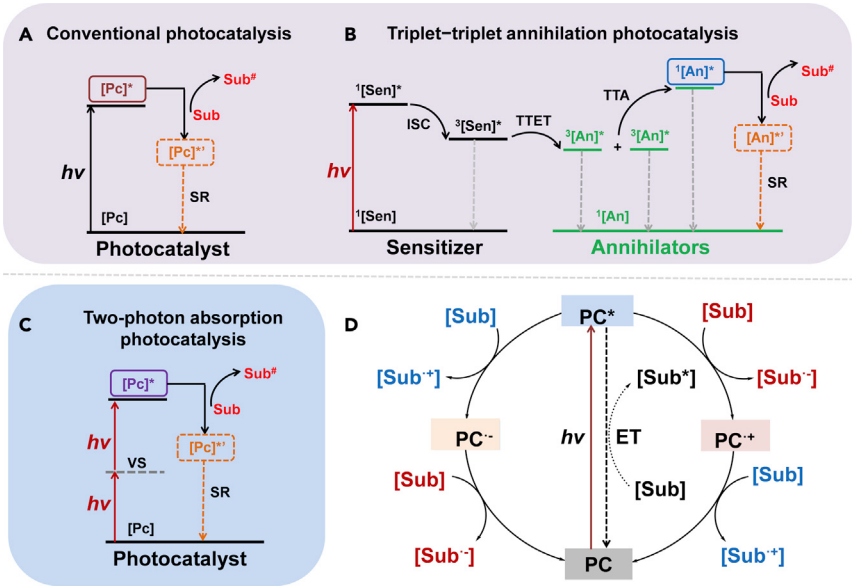

Figure 1. Schematic illustrations of photocatalysis pathways

(A) Conventional one-photon absorption photocatalysis.

(B) Triplet−triplet annihilation photocatalysis.

(C) Two-photon absorption photocatalysis.

(D) Possible photocatalytic pathways. Note: hv, light irradiation; Pc, photocatalyst; Sub, substrate; SR, sacrificial reagent; ISC, intersystem crossing; TTET, triplet-triplet energy transfer; TTA, triplet−triplet annihilation; ET, energy transfer.

ground state. The success of TTA relies on the fine-tuning and intimate interaction of sensitizers and annihilators. Very recently, this TTA strategy has been successfully employed in organic photocatalysis under near-IR light illumination (Ravetz et al., 2019).

In contrast, the TPA strategy requires only one molecule capable of absorbing two low-energy photons simultaneously to generate its excited state. To simplify the overall process and expand the scope of near IR photocatalysis, we reason that it is very attractive to explore TPA photocatalytic systems for organic transformations. In fact, TPA complexes have been investigated in a wide range of applications, including photodynamic therapy (PDT), imaging, sensing, and information storage (Pawlicki et al., 2019; Albota et al., 1998). However, it remains underexplored in organic photocatalysis upon near-IR light irradiation (>700 nm) following the TPA strategy, despite the tremendous interest in organic photocatalysis in recent years. We envision that a TPA complex should be able to drive diverse organic reactions as those outlined in Figure 1D, including redox and energy transfer reactions, as long as the redox potential and/or energy difference could be well matched between the TPA photocatalyst and the substrate of interest. Encouraged by the excellent TPA performance of a ruthenium polypyridyl complex (Ru1, Figure 2A), which can act as a PDT agent under near-IR light radiation (Karges et al., 2020), we decided to synthesize a close analogue of Ru1 and further integrate the resulting ruthenium complex to a metal organic framework (MOF) for the construction of a heterogeneous photocatalyst with molecular TPA sites (MOF-Ru1, Figure 2B). The flexible building units in metal-organic frameworks allow us to incorporate suitable bipyridyl ligands as organic struts which have strong coordination affinity toward ruthenium. Such a design will not only retain the TPA performance of Ru1 but also result in convenient catalyst recycling because of phase separation (Cui et al., 2018; Zhong et al., 2020; Wang et al., 2018; Liang et al., 2017). In fact, catalyst separation and recycling is a long-standing challenge in conventional homogeneous organic photocatalysis.

Herein, we report a ruthenium complex-modified metal-organic framework (MOF-Ru1) as a competent TPA photocatalyst for organic transformations under near-IR light irradiation. Specifically, five kinds of representative organic reactions, including $^1O_2$-involved reactions, reductive, oxidative, and net redox neutral reactions, as well as atom transfer radical polymerization (ATRP), were studied using MOF-Ru1 as the sole photocatalyst upon irradiation at 740 nm under ambient conditions.

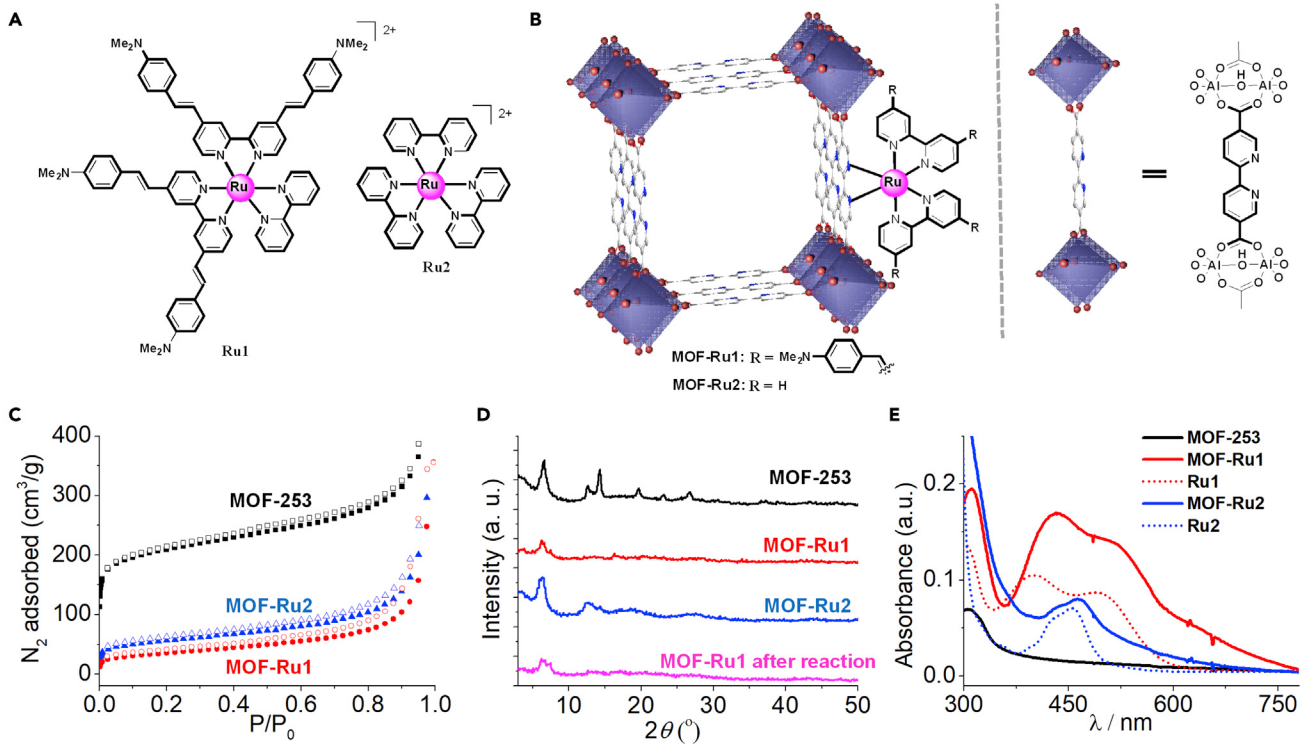

Figure 2. Molecular structures and characterizations

(A) Molecular structures of Ru1 and Ru2.

(B) Representative structures of MOF-Ru1 and MOF-Ru2.

(C) Nitrogen adsorption isotherms of MOF-253 (black), MOF-Ru1 (red), and MOF-Ru2 (blue).

(D) Powder X-ray diffraction (PXRD) patterns of MOF-253, MOF-Ru1, MOF-Ru2, and MOF-Ru1 after reaction.

(E) Steady-state UV/visible absorption spectra of MOF-253, MOF-Ru1, MOF-Ru2, Ru1, and Ru2.

RESULTS AND DISCUSSION

Photocatalyst design, synthesis, and characterization

To craft Ru1, a metal organic framework using 2,2′-bipyridyl ligands as the organic struts is ideal, because post-synthetic modification would enable the convenient coordination of the Ru1 precursor (synthetic details shown in the method details) to the 2,2′-bipyridine units. Therefore, MOF-253, which consists of aluminum oxide clusters and 5,5′-dicaborxyl-2,2′-bipyridyl ligands, was selected as a robust framework to support Ru1(Senkovska et al., 2009). In fact, MOF-253 has been widely utilized in constructing various composites with many applications including catalysis, sensing, and separation(Bloch et al., 2010; Wang et al., 2011; Carson et al., 2012; Zhou et al., 2013; Zhang et al., 2016; Wu et al., 2020). The resulting hybrid composite consisting of MOF-253 and Ru1 was named as MOF-Ru1 (Figure 2B). On the other hand, $[Ru(bpy)_3]^{2+}$ (bpy = 2,2′-bipyridyl, Ru2) is frequently employed as a visible-light photosensitizer for organic photocatalysis following the one-photon absorption mechanism. As a control sample, MOF-253 modified with $[Ru(bpy)_3]^{2+}$ units was also prepared as MOF-Ru2 (Figure 2B). The synthetic details of MOF-R1 and MOF-Ru2 are included in the method details. It should be noted that the TPA cross section of Ru1 is two orders of magnitude higher than that of $[Ru(bpy)_3]^{2+}$(Kargeset al., 2020).

The as-prepared MOF-253 exhibits a large Langmuir surface area (1,625 m^2/g, Figure 2C) and characteristic powder X-ray diffraction (PXRD) pattern (Figure 2D), in good agreement with the reported results (Sun et al., 2015). As expected, the nitrogen adsorption-desorption isotherms indicated that the Langmuir surface area decreased from the pristine MOF sample to MOF-Ru1 (392 m^2/g) and MOF-Ru2 (638 m^2/g). The surface area decrease can be attributed to the partial occupancy within MOF channels by ruthenium species, wherein larger Ru1 led to the smaller surface area of MOF-Ru1 relative to that of MOF-Ru2. In addition, the corresponding pore size distribution curves of MOF-253, MOF-Ru1, and MOF-Ru2 (Figure S1) indicated that the microporous size distribution is about 1–2 nm. Upon the coordination of those ruthenium

complexes, the PXRD patterns of MOF-Ru1 and MOF-Ru2 still present the characteristic diffraction peaks resulting from MOF-253, albeit with lower intensity probably because of the decreased crystallinity. The relative ratio of Ru/Al was obtained from inductively coupled plasma – optical emission spectroscopy (ICP-OES) measurements, which revealed the Ru/Al molar ratio of 2.1 and 7.4% for MOF-Ru1 and MOF-Ru2, respectively. As shown in Figure S2, the SEM image of MOF-Ru1 demonstrates that it retains similar long-flake morphology as that of the parent MOF-253.

Without the coordination of ruthenium complexes, the parent MOF-253 does not present appreciable absorption in the visible region (Figure 2E). However, because of the metal/ligand-to-ligand charge transfer (ML-LCT) transitions in Ru1, MOF-Ru1 exhibits a visible-light absorption band at 400–600 nm, which roughly resembles those obtained from Ru1 (Figure 2D). Comparatively, Ru2 and MOF-Ru2 show similar absorption in 400–550 nm. Despite great efforts, our attempt to determine the TPA cross section of MOF-Ru1 was yet successful, partially because of its weak emission (690–740 nm, Figure S3) with a maximum located in proximity to the excitation light wavelength of interest (740 nm). As previously reported, Ru1 shows an exceptionally strong TPA performance with the maximum absorption band within 720–800 nm (Karges et al., 2020). We thus explored its catalytic performance for near-IR light-driven organic transformations using 740 nm LED as the light source (see photocatalysis details in the method details).

Photocatalytic performance evaluation: C–N coupling of benzylamines

To evaluate the photocatalytic performance of MOF-Ru1 under NIR light irradiation, our initial investigations were focused on the oxidative C-N coupling of benzylamine and its derivatives to imines, which could be driven by $^1O_2$ (Prier et al., 2013; Skubi et al., 2016; Wang et al., 2016; Li et al., 2019; Huang et al., 2020). The *in situ* formation of $^1O_2$ is an energy transfer process. Specifically, upon irradiation, triplet-triplet energy transfer takes place between the excited MOF-*Ru1 and O_2 to generate $^1O_2$, which is further involved in the oxidative C-N coupling of benzylamines. As shown in Figure 3A, MOF-Ru1 was able to convert benzylamine to the imine product with a yield of 53% within 3 h irradiation at 740 nm (entry 1). As a comparison, using the parent MOF-253 (entry 2) or MOF-Ru2 (entry 3) as the photocatalyst resulted in negligible imine yield under the same condition, highlighting the importance of two-photon absorption capability of MOF-Ru1 in this reaction. A nonlinear relationship between the yield of benzyl amine C-N coupling product and the LED power was observed (Figures S4 and S5), in agreement with the TPA nature of MOF-Ru1 as the photosensitizer (Li et al., 2019; Glaser et al., 2020; Glaser and Wenger, 2020). Furthermore, the presence of NaN_3 (entry 4), a $^1O_2$ quencher, could substantially suppress the formation of the imine product with a yield as low as 5% under the same condition, further corroborating the critical role played by $^1O_2$ in the C-N coupling of benzylamine. As anticipated, control experiments conducted in the absence of O_2 (entry 5), in the dark (entry 6), or without photocatalyst (entry 7) did not form any desirable product. The ruthenium loading experiments indicated that the higher loading of ruthenium contributes to the better photocatalytic performance (Table S1 and Figure S6). The structure and chemical composition of MOF-Ru1 after one cycle of reaction was investigated by using scanning electron microscopy and nitrogen adsorption analysis (Figures S7 and S8), which showed the similar long-flake morphology, Langmuir surface area (356 m^2/g), and pore size distribution (one to two nm) relative to the pristine MOF-Ru1.

Monitoring the product evolution over photocatalysis duration indicated that a nearly quantitative yield of the desirable imine product could be achieved within 7 h irradiation at 740 nm (Figure 3B). The recoverability and reusability of MOF-Ru1 were also evaluated via the recycling experiments, thanks to the facile separation of the photocatalyst by centrifugation. As shown in Figure 3C, MOF-Ru1 maintained high activity for the first four consecutive photocatalysis cycles (yield >90%). Such a $^1O_2$-driven C-N coupling transformation was next expanded to various benzylamine derivatives. As summarized in Figure 3D, regardless of the presence of electron-donating or electron-withdrawing groups, MOF-Ru1 was able to produce the anticipated imine products with excellent yields (>90%) under 740 nm irradiation for 5 h. Even using 2-thiophenemethylamine (1i) as the organic substrate, the anticipated C-N coupling product 2i was also produced with a 91% yield.

The generality of MOF-Ru1 as a TPA photocatalyst toward other reactions was then investigated for a number of organic transformations, such as reductive hydrodehalogenation of α-bromoketones, oxidative hydroxylation of arylboronic acids, net redox neutral cyanation of tetrahydroisoquinoline, and atom transfer radical polymerization of methyl methacrylate.

A

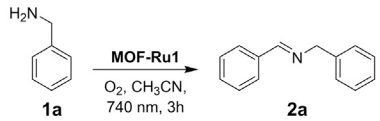

Entry	Deviation from the default condition	Yield (%)
1	Default[a]	56
2	Use MOF-253 as the photocatalyst	n.d.
3	Use MOF-Ru2 as the photocatalyst	7
4	With 2 eq NaN_3	5
5	No O_2	n.d.
6	No light irradiation	n.d.
7	No photocatalyst	n.d.

B

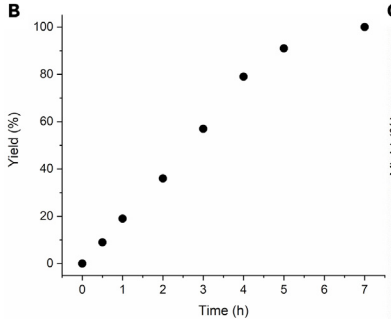

C

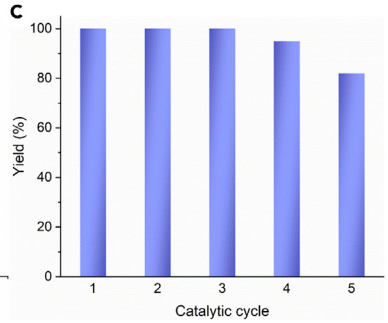

D

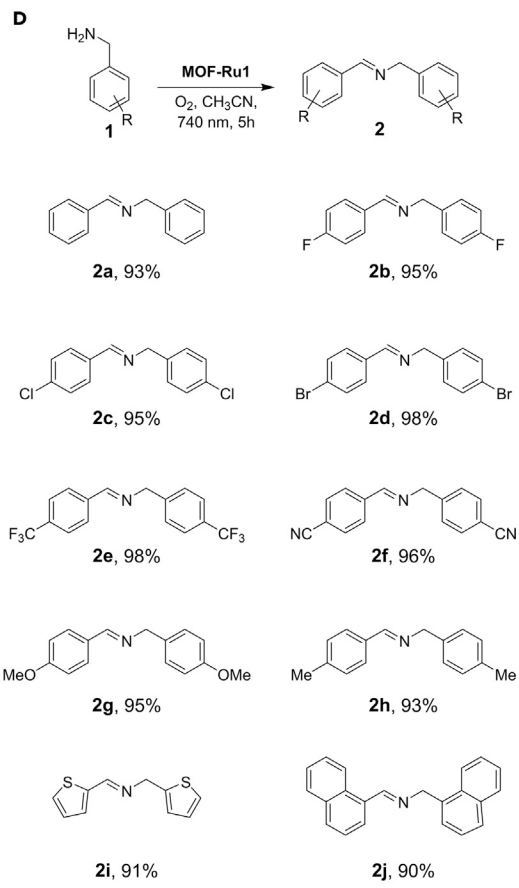

Figure 3. Control experiments and NIR photocatalytic C-N coupling of benzylamines

(A) Table summarizing C-N coupling reaction of benzylamine. [a]All reactions were performed by using 1a (0.10 mmol), photocatalyst, aerated CH_3CN (2 mL) under 740 nm light irradiation at room temperature for 3 h. The yields were determined by ^1H NMR analysis using 3,4,5-trimethoxybenzaldehyde as an internal standard.

(B) Time-dependent photocatalytic transformation.

(C) Photocatalytic recycling experiments (The reactions were performed for 7 h.).

(D) Evaluating the scope of the photocatalytic C-N coupling of benzylamine derivatives (See details in the method details).

Hydrodehalogenation of α-bromoketones

Hydrodehalogenation of α-bromoketones was selected as a representative reaction for reductive photocatalysis. Under visible light irradiation, $[Ru(bpy)_3]^{2+}$ could be employed as an effective photocatalyst to drive the hydrodehalogenation of α–bromoketones when 9,10-dihydro-10-methylacridine is used as the terminal reductant (Fukuzumi et al., 1990). However, no product could be detected using $[Ru(bpy)_3]^{2+}$ as the photocatalyst when the irradiation wavelength was 740 nm. Recently, excited Eosin Y, following triplet-fusion upconversion was demonstrated to realize the hydrodehalogenation of α-bromoketones upon near-IR light irradiation, albeit an organic annihilator was also required (Majek et al., 2015). Herein, we used MOF-Ru1 as a TPA-active NIR photocatalyst to perform the above reaction. To our delight, α-bromoketones underwent hydrodehalogenation smoothly in the presence of MOF-Ru1 (1.0 mol % Ru relative to the organic substrate amount) under 740 nm light irradiation in deaerated acetonitrile when triethanolamine (TEOA) was used as the sacrificial electron/proton donor. The target product were unable to be detected without 740 nm light irradiation or using $[Ru(bpy)_3](PF_6)_2$ as photocatalyst. As shown in Figure 4A, high yields (>80%) could be obtained for a variety of α-bromoketones bearing either electron-withdrawing (-F, -Cl, -Br, -CN, $-NO_2$) or electron-donating (-OMe) groups. The sterically hindered substrate 2-bromo-1-(2-naphthalenyl)ethanone (3 h) could also be transformed to the anticipated product with an isolated yield of 89%. Furthermore, an excellent selectivity of hydrodebromination was observed for 2-bromo-1-(4-bromophenyl)ethanone (1e), wherein only the desirable product 4e

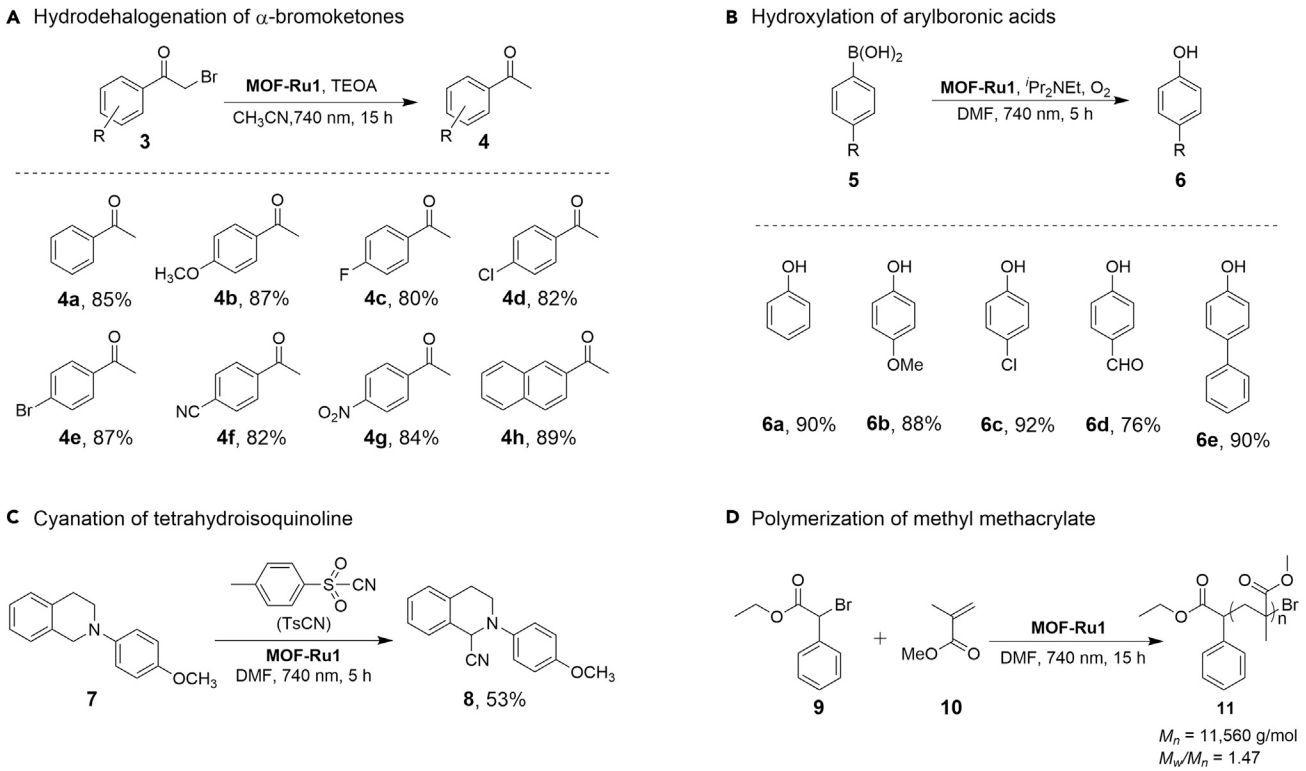

Figure 4. Evaluating the scope of NIR photocatalysis

(A) Photocatalytic hydrodehalogenation of α-bromoketones in deaerated CH_3CN using MOF-Ru1 and TEOA upon irradiation at 740 nm for 15 h at room temperature.

(B) Photocatalytic hydroxylation of arylboronic acids in O_2-saturated DMF using MOF-Ru1 and $^{i}Pr_2NEt$ upon irradiation at 740 nm for 5 h at room temperature.

(C) Photocatalytic C-H cyanation of tetrahydroisoquinoline in deaerated DMF using MOF-Ru1 and TsCN upon irradiation at 740 nm for 5 h at room temperature.

(D) Photocatalytic polymerization of methyl methacrylate using MOF-Ru1 and ethyl α-bromobenzeneacetate upon irradiation at 740 nm for 15 h at room temperature.

was yielded (87%). Control experiments demonstrated that no hydrodehalogenation product was formed in the absence of MOF-Ru1 or 740 nm light irradiation. Regarding the photocatalytic cycle, the excited MOF-$*Ru^{II}$1 is reductively quenched by TEOA to form MOF-Ru^{I}1, which is able to reduce α-bromoketones to α-ketomethyl radical and simultaneously release a bromide anion. After further acceptance of an electron and a proton, the intermediate α-ketomethylradical is transformed to the final product, acetophenone.

Hydroxylation of arylboronic acids

O_2 is widely regarded as a green oxidant in organic synthesis. Following one-electron reduction by an excited photocatalyst such as $*[Ru(bpy)_3]^{2+}$, the *in situ* formed superoxide radical anion ($O_2^{\bullet-}$) from O_2 is a powerful oxidant which is able to drive the hydroxylation of arylboronic acids to yield corresponding phenols(Zou et al., 2012; Yu and Cohen, 2015). When MOF-Ru1 was employed as the photocatalyst with a low Ru amount (1.0 mol% Ru relative to the organic substrate amount), 740 nm light irradiation was adequate to initiate the oxidation of various arylboronic acids to their corresponding phenols in aerated dimethylformamide (DMF). This reaction was unable to proceed without 740 nm light irradiation or using $[Ru(bpy)_3](PF_6)_2$ as a photocatalyst. In this case, *N,N*-diisopropylethylamine ($^{i}Pr_2NEt$) was employed as the sacrificial electron donor. As shown in Figure 4B, decent amounts of isolated yields (76–92%) were achieved for different arylboronic acids regardless of the presence of electron-rich/withdrawing substituents at the para position of the phenyl rings. Analogous to the previous mechanism of hydrodehalogenation, this catalytic cycle starts with the formation of MOF-Ru^{I}1 after its reductive quenching by $^{i}Pr_2NEt$. MOF-Ru^{I}1 is able to reduce O_2 to form $O_2^{\bullet-}$ which is responsible for the subsequent hydroxylation of arylboronic acids.

Cyanation of tetrahydroisoquinoline

In contrast to the above two types of photocatalytic reactions, which require sacrificial reagents, redox neutral reactions possess the possibility to utilize both the reduction and oxidation power of a photocatalyst, maximizing the energy efficiency and atom economy of photocatalysis. Within this context, we decided to explore the performance of MOF-Ru1 toward the C-H cyanation of tetrahydroisoquinoline, which is a net redox neutral reaction (Ide et al., 2018). As shown in Figure 4C, the cyanation of *N*-(4-methoxy-phenyl)-1,2,3,4-tetrahydroisoquinoline (7) underwent smoothly in DMF under 740 nm light irradiation to afford product 8 with a 53% isolated yield using MOF-Ru1 as the sole photocatalyst. The control experiments indicated that no detectable product was formed under the condition of lacking 740 nm light irradiation or using $[Ru(bpy)_3](PF_6)_2$ as a photocatalyst. In this reaction, *p*-toluenesulfonyl cyanide (TsCN) is employed as the cyanide source, which is able to oxidatively quench the excited MOF-*Ru1 to generate a cyanide anion, a sulfonyl radical, and MOF-Ru^{III}1. Subsequently, MOF-Ru^{III}1 would oxidize 7 to yield an aminium radical cation. Following α-H deprotonation, a neutral carbon radical intermediate is formed, which might react with the sulfonyl radical to form an iminium cation. A nucleophilic attack of the cyanide anion to the iminium cation will furnish the formation of the final cyanation product. Overall, such a catalytic cycle takes advantage of two single-electron transfer processes, utilizing not only the reducing power of MOF-*Ru^{II}1 but also the oxidizing capability of MOF-Ru^{III}1 and hence circumventing the necessity of sacrificial reagents.

Atom transfer radical polymerization of methyl methacrylate

Encouraged by the competent reducing power of MOF-Ru^{I}1 in the above hydrodehalogenation of α-bromoketones, we decided to further expand its utilization toward photo-induced polymerization, such as atom transfer radical polymerization of methyl methacrylate (MMA), wherein reductive C-Br bond cleavage is the initial step (Fors and Hawker, 2012). Specifically, ethyl α-bromobenzeneacetate (9) was utilized as the initiator. To our delight, simple irradiation at 740 nm using MOF-Ru1 as the sole photocatalyst and $^{i}Pr_2NEt$ as the sacrificial electron donor resulted in steady MMA polymerization (Figure 4D). Gel permeation chromatography analysis (Figure S9) provided the molecular weight (M_n) of 11,560 g mol^{-1} and dispersity (M_w/M_n) of 1.47 for the obtained poly(methyl methacrylate) (PMMA) product. It is worth mentioning that the corresponding polymerized product was not observed by using $[Ru(bpy)_3](PF_6)_2$ as a photocatalyst or without 740 nm light irradiation.

Conclusions

We have developed a hybrid metal-organic framework photocatalyst integrated with a TPA-active ruthenium motif, MOF-Ru1, which is able to catalyze a diverse array of organic transformations under 740 nm light irradiation. Representative photocatalytic organic reactions including $^1O_2$-driven C-N coupling of benzylamines, redox reactions, and ATRP polymerization were all successfully executed using MOF-Ru1 as the sole photocatalyst upon near IR light irradiation. We envision these results will facilitate the development of advanced photocatalytic systems following the two-photon absorption strategy for the utilization of low-energy photons, especially in the near IR region.

Limitations of the study

Two-photon-absorbing (TPA) photocatalysis provides a straightforward strategy for utilizing near-infrared low-energy photons. The two-photon absorption properties of the TPA photocatalysts play a vital role in the specific catalytic performance. The accurate determination of the two-photon absorption cross-section for TPA photocatalysts is able to aid in the understanding of the mechanistic aspects for the reactions. However, the current heterogeneous MOF-Ru photocatalyst shows strong two-photon absorption but weak emission, which leads to the challenge of measuring its two-photon absorption cross-section value. The future work will focus on rationalizing the structure of TPA photocatalysts, unveiling the details of the reaction mechanism and expanding the reaction scope.

STAR★METHODS

Detailed methods are provided in the online version of this paper and include the following:

- KEY RESOURCES TABLE
- RESOURCE AVAILABILITY
  - Lead contact
  - Materials availability

SUPPLEMENTAL INFORMATION

Supplemental information can be found online at https://doi.org/10.1016/j.isci.2022.104064.

ACKNOWLEDGMENTS

We acknowledge the financial support of the National Science Foundation (CHE1955358) and the University of Cincinnati.

AUTHOR CONTRIBUTIONS

J. T., G. H., and Y. S. envisioned and designed the project. J. T., G. H., G. L., and K. Y. conducted the methodology development, synthesis, and characterization of compounds. Y. S. supervised the project. All authors contributed to the discussion of experimental results. The manuscript was written by all contributing authors.

DECLARATION OF INTERESTS

The authors declare no competing financial interest. J. T. is currently a postdoctoral fellow at Northwestern University with no competing interests.

Received: October 13, 2021
Revised: December 23, 2021
Accepted: March 9, 2022
Published: April 15, 2022

REFERENCES

Albota, M., Beljonne, D., Brédas, J.-L., Ehrlich, J.E., Fu, J.-Y., Heikal, A.A., Hess, S.E., Kogej, T., Levin, M.D., and Marder, S.R. (1998). Design of organic molecules with large two-photon absorption cross sections. Science *281*, 1653–1656.

Bloch, E.D., Britt, D., Lee, C., Doonan, C.J., Uribe-Romo, F.J., Furukawa, H., Long, J.R., and Yaghi, O.M. (2010). Metal insertion in a microporous meta-organic framework lined with 2, 2′-bipyridine. J. Am. Chem. Soc. *132*, 14382–14384.

Buzzetti, L., Crisenza, G.E., and Melchiorre, P. (2019). Mechanistic studies in photocatalysis. Angew. Chem. Int. Ed. *58*, 3730–3747.

Caputo, J.A., Frenette, L.C., Zhao, N., Sowers, K.L., Krauss, T.D., and Weix, D.J. (2017). General and efficient C–C bond forming photoredox catalysis with semiconductor quantum dots. J. Am. Chem. Soc. *139*, 4250–4253.

Carson, F., Agrawal, S., Gustafsson, M., Bartoszewicz, A., Moraga, F., Zou, X., and Martin-Matute, B. (2012). Ruthenium complexation in an aluminium metal-organic framework and its application in alcohol oxidation catalysis. Chem. Eur. J. *18*, 15337–15344.

Ciamician, G. (1912). The photochemistry of the future. Science *36*, 385–394.

Cui, X., Li, W., Ryabchuk, P., Junge, K., and Beller, M. (2018). Bridging homogeneous and heterogeneous catalysis by heterogeneous single-metal-site catalysts. Nat. Catal. *1*, 385–397.

Dolgopolova, E.A., Rice, A.M., Martin, C.R., and Shustova, N.B. (2018). Photochemistry and photophysics of MOFs: steps towards MOF-based sensing enhancements. Chem. Soc. Rev. *47*, 4710–4728.

Fallon, K.J., Churchill, E.M., Sanders, S.N., Shee, J., Weber, J.L., Meir, R., Jockusch, S., Reichman, D.R., Sfeir, M.Y., and Congreve, D.N. (2020). Molecular engineering of chromophores to enable triplet-triplet annihilation upconversion. J. Am. Chem. Soc. *142*, 19917–19925.

Fors, B.P., and Hawker, C.J. (2012). Control of a living radical polymerization of methacrylates by light. Angew. Chem. Int. Ed. *124*, 8980–8983.

Fukuzumi, S., Mochizuki, S., and Tanaka, T. (1990). Photocatalytic reduction of phenacyl halides by 9, 10-dihydro-10-methylacridine: control between the reductive and oxidative quenching pathways of tris (bipyridine) ruthenium complex utilizing an acid catalysis. J. Phys. Chem. *94*, 722–726.

Glaser, F., Kerzig, C., and Wenger, O.S. (2020). Multi-photon excitation in photoredox catalysis: concepts, applications, methods. Angew. Chem. Int. Ed. *59*, 10266–10284.

Glaser, F., and Wenger, O.S. (2020). Recent progress in the development of transition-metal based photoredox catalysts. Coord. Chem. Rev. *405*, 213129.

Günes, S., Neugebauer, H., and Sariciftci, N.S. (2007). Conjugated polymer-based organic solar cells. Chem. Rev. *107*, 1324–1338.

Huang, Y., Liu, C., Li, M., Li, H., Li, Y., Su, R., and Zhang, B. (2020). Photoimmobilized Ni clusters boost photodehydrogenative coupling of amines to imines via enhanced hydrogen evolution kinetics. ACS Catal. *10*, 3904–3910.

Ide, T., Shimizu, K., Egami, H., and Hamashima, Y. (2018). Redox-neutral C–H cyanation of tetrahydroisoquinolines under photoredox catalysis. Tetrahedron Lett. *59*, 3258–3261.

Karges, J., Kuang, S., Maschietto, F., Blacque, O., Ciofini, I., Chao, H., and Gasser, G. (2020). Rationally designed ruthenium complexes for 1-and 2-photon photodynamic therapy. Nat. Commun. *11*, 1–13.

Kisch, H. (2017). Semiconductor photocatalysis for chemoselective radical coupling reactions. Acc. Chem. Res. *50*, 1002–1010.

Liang, J., Liang, Z., Zou, R., and Zhao, Y. (2017). Heterogeneous catalysis in zeolites, mesoporous silica, and metal–organic frameworks. Adv. Mater. *29*, 1701139.

Li, H., Yang, Y., He, C., Zeng, L., and Duan, C. (2019). Mixed-ligand metal–organic framework for two-photon responsive photocatalytic C–N and C–C coupling reactions. ACS Catal. *9*, 422–430.

Li, X.-B., Xin, Z.-K., Xia, S.-G., Gao, X.-Y., Tung, C.-H., and Wu, L.-Z. (2020). Semiconductor nanocrystals for small molecule activation via artificial photosynthesis. Chem. Soc. Rev. *49*, 9028–9056.

Majek, M., Faltermeier, U., Dick, B., Pérez-Ruiz, R., and Jacobi von Wangelin, A. (2015). Application of visible-to-UV photon upconversion to photoredox catalysis: the activation of aryl bromides. Chem. Eur. J. *21*, 15496–15501.

Nicewicz, D.A., and MacMillan, D.W. (2008). Merging photoredox catalysis with organocatalysis: the direct asymmetric alkylation of aldehydes. Science *322*, 77–80.

Park, Y.I., Lee, K.T., Suh, Y.D., and Hyeon, T. (2015). Upconverting nanoparticles: a versatile platform for wide-field two-photon microscopy and multi-modal in vivo imaging. Chem. Soc. Rev. *44*, 1302–1317.

Pawlicki, M., Collins, H.A., Denning, R.G., and Anderson, H.L. (2019). Two-photon absorption and the design of two-photon dyes. Angew. Chem. Int. Ed. *48*, 3244–3266.

Prier, C.K., Rankic, D.A., and MacMillan, D.W. (2013). Visible light photoredox catalysis with transition metal complexes: applications in organic synthesis. Chem. Rev. *113*, 5322–5363.

Ravetz, B.D., Pun, A.B., Churchill, E.M., Congreve, D.N., Rovis, T., and Campos, L.M. (2019). Photoredox catalysis using infrared light via triplet fusion upconversion. Nature *565*, 343–346.

Schultz, D.M., and Yoon, T.P. (2014). Solar synthesis: prospects in visible light photocatalysis. Science *343*, 1239176.

Senkovska, I., Hoffmann, F., Froba, M., Getzschmann, J., Bohlmann, W., and Kaskel, S. (2009). New highly porous aluminium based metal-organic frameworks: Al(OH)(ndc) (ndc=2,6-naphthalene dicarboxylate) and Al(OH)(bpdc) (bpdc=4,4′-biphenyl dicarboxylate). Microp. Mesopor. Mat. *122*, 93–98.

Skubi, K.L., Blum, T.R., and Yoon, T.P. (2016). Dual catalysis strategies in photochemical synthesis. Chem. Rev. *116*, 10035–10074.

Sun, D., Gao, Y., Fu, J., Zeng, X., Chen, Z., and Li, Z. (2015). Construction of a supported Ru complex on bifunctional MOF-253 for photocatalytic CO_2 reduction under visible light. Chem. Commun. *51*, 2645–2648.

Twilton, J., Zhang, P., Shaw, M.H., Evans, R.W., and MacMillan, D.W. (2017). The merger of transition metal and photocatalysis. Nat. Rev. Chem. *1*, 0052.

Wang, A., Li, J., and Zhang, T. (2018). Heterogeneous single-atom catalysis. Nat. Rev. Chem. *2*, 65–81.

Wang, C., Xie, Z., deKrafft, K.E., and Lin, W. (2011). Doping metal–organic frameworks for water oxidation, carbon dioxide reduction, and organic photocatalysis. J. Am. Chem. Soc. *133*, 13445–13454.

Wang, H., Jiang, S., Chen, S., Li, D., Zhang, X., Shao, W., Sun, X., Xie, J., Zhao, Z., and Zhang, Q. (2016). Enhanced singlet oxygen generation in oxidized graphitic carbon nitride for organic synthesis. Adv. Mater. *28*, 6940–6945.

Wu, S., Min, H., Shi, W., and Cheng, P. (2020). Multicenter metal-organic framework-based ratiometric fluorescent sensors. Adv. Mater. *32*, 1805871.

Yoon, T.P., Ischay, M.A., and Du, J. (2010). Visible light photocatalysis as a greener approach to photochemical synthesis. Nat. Chem. *2*, 527–532.

Yu, X., and Cohen, S.M. (2015). Photocatalytic metal–organic frameworks for the aerobic oxidation of arylboronic acids. Chem. Commun. *51*, 9880–9883.

Zhang, L., Ran, J., Qiao, S.-Z., and Jaroniec, M. (2019). Characterization of semiconductor photocatalysts. Chem. Soc. Rev. *48*, 5184–5206.

Zhang, W., Li, B., Ma, H., Zhang, L., Guan, Y., Zhang, Y., Zhang, X., Jing, P., and Yue, S. (2016). Combining ruthenium(II) complexes with metal-organic frameworks to realize effective two-photon absorption for singlet oxygen generation. ACS Appl. Mater. Interfaces *8*, 21465–21471.

Zheng, Z., Zhang, T., Liu, H., Chen, Y., Kwok, R.T., Ma, C., Zhang, P., Sung, H.H., Williams, I.D., and Lam, J.W. (2018). Bright near-infrared aggregation-induced emission luminogens with strong two-photon absorption, excellent organelle specificity, and efficient photodynamic therapy potential. ACS Nano *12*, 8145–8159.

Zhong, J., Yang, X., Wu, Z., Liang, B., Huang, Y., and Zhang, T. (2020). State of the art and perspectives in heterogeneous catalysis of CO_2 hydrogenation to methanol. Chem. Soc. Rev. *49*, 1385–1413.

Zhou, J., Liu, Q., Feng, W., Sun, Y., and Li, F. (2015). Upconversion luminescent materials: advances and applications. Chem. Rev. *115*, 395–465.

Zhou, L., Liu, Z., Guan, Z., Tian, B., Wang, L., Zhou, Y., Zhou, Y., Lei, J., Zhang, J., and Liu, Y. (2020). 0D/2D plasmonic $Cu_{2-x}S$/g-C_3N_4nanosheets harnessing UV-vis-NIR broad spectrum for photocatalytic degradation of antibiotic pollutant. Appl. Catal. B *263*, 118326.

Zhou, T., Du, Y., Borgna, A., Hong, J., Wang, Y., Han, J., Zhang, W., and Xu, R. (2013). Post-synthesis modification of a metal–organic framework to construct a bifunctional photocatalyst for hydrogen production. Energy Environ. Sci. *6*, 3229–3234.

Zou, Y.Q., Chen, J.R., Liu, X.P., Lu, L.Q., Davis, R.L., Jørgensen, K.A., and Xiao, W.J. (2012). Highly efficient aerobic oxidative hydroxylation of arylboronic acids: photoredox catalysis using visible light. Angew. Chem. Int. Ed. *124*, 808–812.

STAR★METHODS

KEY RESOURCES TABLE

REAGENT or RESOURCE	SOURCE	IDENTIFIER
Chemicals, peptides, and recombinant proteins		
4,4′-Dimethyl-2,2′-dipyridyl	Sigma-Aldrich	CAS:1134-35-6
Potassium tert-butoxide	Sigma-Aldrich	CAS:865-47-4
4-(dimethylamino) benzaldehyde	Sigma-Aldrich	CAS:100-10-7
Tetrakis(dimethylsulfoxide) dichlororuthenium(II)	Sigma-Aldrich	CAS:89395-66-4
Lithium chloride	Sigma-Aldrich	CAS:7447-41-8
2,2′-bipyridine	Sigma-Aldrich	CAS: 366-18-7
Dimethylformamide	Sigma-Aldrich	CAS: 68-12-2
Ammonium hexafluorophosphate	Sigma-Aldrich	CAS:1120-48-5
Benzylamine	Sigma-Aldrich	CAS:100-46-9
4-Fluorobenzylamine	Sigma-Aldrich	CAS:140-75-0
Methanol	Sigma-Aldrich	CAS:67-56-1
Hexane	Sigma-Aldrich	CAS:110-54-3
2-Bromoacetophenone	Sigma-Aldrich	CAS:70-11-1
2-Bromo-4′-methoxyacetophenone	Sigma-Aldrich	CAS: 2632-13-5
2-Bromo-4′-fluoroacetophenone	Sigma-Aldrich	CAS: 403-29-2
Triethanolamine	Sigma-Aldrich	CAS:102-71-6
Phenylboronic acid	Ambeed, Inc.	CAS: 98-80-6
N,N-Diisopropylethylamine	Sigma-Aldrich	CAS: 7087-68-5
1,2,3,4-Tetrahydroisoquinoline	Sigma-Aldrich	CAS: 91-21-4
4-Iodoanisole	Sigma-Aldrich	CAS: 696-62-8
Copper(I) iodide	Sigma-Aldrich	CAS: 7681-65-4
p-Toluenesulfonyl cyanide	Sigma-Aldrich	CAS: 19158-51-1
Methyl methacrylate	Sigma-Aldrich	CAS: 80-62-6
Ethyl α-bromophenylacetate	Sigma-Aldrich	CAS: 2882-19-1

RESOURCE AVAILABILITY

Lead contact

Further information and requests for resources and reagents should be directed to and will be fulfilled by the lead contact, Yujie Sun (yujie.sun@uc.edu).

Materials availability

All data supporting the newly synthesized compounds can be found within the manuscript and the supplemental information or can be received from the lead contact upon request.

Data and code availability

- Any additional information required to reanalyze the data reported in this paper is available from the lead contact upon request. Data: All data reported in this paper will be shared by the lead contact upon request.
- Code: This paper does not report original code.
- Any additional information required to reanalyze the data reported in this paper is available from the lead contact upon request.

METHOD DETAILS

General reagent information

All starting materials were purchased from commercial vendors and used as received without further purification unless otherwise noted.

General analytical information

^{1}H NMR and ^{13}C NMR spectra were recorded in the designated solvents on a Bruker AV 400 MHz spectrometer. Mass analysis was performed using Thermo Orbitrap Fusion Lumos instrument. The Al and Ru quantities of each sample were analyzed via inductively coupled plasma mass spectrometry (ICP-MS, Agilent 7500ce) in 2% nitric acid, equipped with micromist quartz nebulizer, 2.5 mm ID quartz torch with Pt shield torch, Pt sampler and skimmer cones. The powder X-ray diffraction (PXRD) analyses were conducted with a PANalytical Empyrean diffractometer, operated at 45 kV and 40 mA (scanning step: 0.1° per step). Scanning electron microscopy (SEM, FEI XL30, 15 kV)was used to image the samples. The surface area measurements were carried out by measuring the N_2 adsorption/desorption isotherms on an automated gas sorption analyzer (Quantachrome Instruments).Absorption spectra were collected on an Agilent 8454 UV-Vis Spectrophotometer. MOF-253and $[Ru(bpy)_3]Cl_2$ (bpy2,2′-bipyridyl) were synthesized as previously described. 740 nm LEDs were purchased from Kessil and the information is shown as followings.

PR160L-740-C

Radiant Flux (optical output): 8,180 mW

Intensity at 1 cm from light: 308.43 mW/cm^2

Power Consumption: Max. 30 W

730 nm LEDs were purchased from Thorlabs and the information is shown as followings.

M730L5

LED output power (typical): 680 mW

Maximum irradiation at 2 cm from light: 13.1 μW/mm^2

The power of M730L5 was finely tuned by the LED driver (Thorlabs, DC2200).

Syntheses and characterizations

Synthesis of (E,E′)-4,4′-Bis[p-(N,N-dimethylamino)styryl]-2,2′-bipyridine (L)

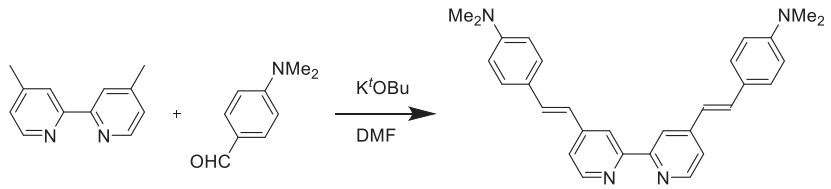

(*E,E′*)-4,4′-Bis[*p*-(*N,N*-dimethylamino)styryl]-2,2′-bipyridine was prepared according to the reported literature with some modifications. The solution of 4,4′-dimethyl-2,2′-bipyridine(0.92 g, 5 mmol) and K^{t}OBu (2.3 g, 20 mmol) in dry DMF (100 mL)was stirred for 2 h under argon atmosphere. 4-(dimethylamino) benzaldehyde (2.2 g, 15 mmol) was then added to the reaction mixture. The resulting mixture was heated at 90°C for15 h. After cooling to room temperature, the solution was treated with 400 mL deionized water and the suspension was stored at room temperature for additional 5 h. The precipitated solid was filtered and washed with water, diethyl ether, and dichloromethane to afford 1.6 g yellow solid product (Yield: 73%).

^{1}H-NMR (400 MHz, $CDCl_3$): δ 8.61 (d, *J* = 5.0 Hz, 2H), 8.48 (s, 2H), 7.34 - 7.48 (m, overlapped,8H), 6.91 (d, *J* = 16 Hz, 2H), 6.72 (d, *J* = 8.6 Hz, 4H), 3.02 (s, 12H).

Synthesis of [Ru(2,2′-bipyridine)((E,E′)-4,4′-Bis[p-(N,N-dimethylamino)styryl]-2,2′-bipyridine)$_2$] [PF_6]$_2$ (Ru1)

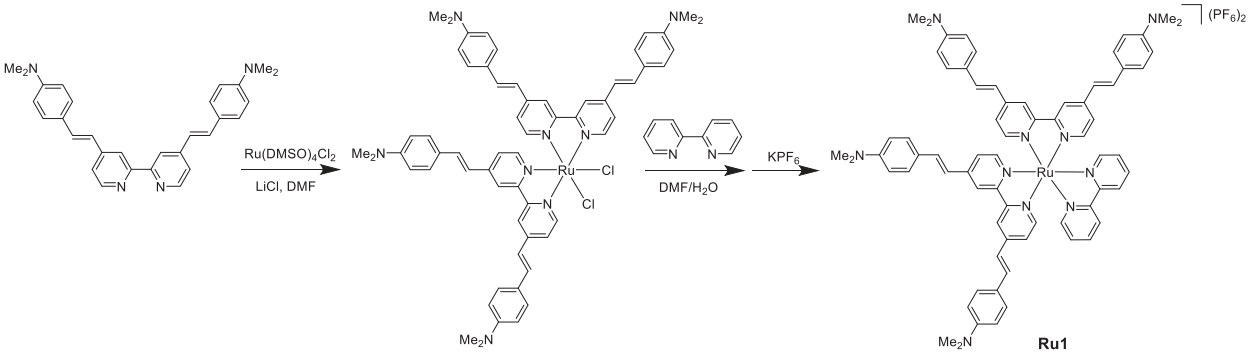

[Ru(2,2′-bipyridine)((*E,E*′)-4,4′-Bis[*p*-(*N,N*-dimethylamino)styryl]-2,2′ bipyridine)$_2$][PF_6]$_2$(Ru1) was prepared according to the reported literature with some modifications. A mixture of (*E,E*′)-4,4′-Bis[*p*-(*N,N*-dimethylamino)styryl]-2,2′-bipyridine (L, 223 mg, 0.5 mmol),Ru(DMSO)$_4$Cl$_2$ (121 mg, 0.25 mmol), and lithium chloride (1.06 g, 25 mmol) in dry DMF (30 mL)was refluxed for 5 h under argon atmosphere. The solution was then cooled down to room temperature and water (200 mL) was added. The solid precipitate was filtered and washed with water and diethyl ether to give the intermediate compound of [Ru((*E,E*′)-4,4′-Bis[*p*-(*N,N*-dimethylamino)styryl]-2,2′-bipyridine)$_2$Cl$_2$] (RuL_2Cl_2) without further purification. RuL_2Cl_2 (107 mg, 0.1 mmol) and 2,2′-bipyridine(24 mg, 0.15 mmol) were suspended in DMF/H_2O (v/v, 30/30 mL). The mixture was then refluxed at 100°C for 8 h under argon atmosphere. After cooling to room temperature, the solvent was removed under reduced pressure. The residue was dissolved in methanol and added with a saturated aqueous solution of NH_4PF_6. The dark-brown precipitated solid product (Ru1) was filtered and washed with water and diethyl ether and a yield of 86% (124 mg) was obtained. ^{1}H NMR (400 MHz, CD_3CN): δ8.61 (s, 4H), 8.48 (d, *J* = 8.4 Hz, 2H), 8.02 (t, *J* = 7.8 Hz, 2H),7.86 (d, *J* = 5.3 Hz,2H), 7.63 - 7.68 (m, overlapped,6H), 7.50 - 7.54 (m, overlapped,10H),7.34 - 7.42 (m, overlapped,6H), 7.01 (d, *J* = 16 Hz, 4H), 6.77 - 6.80 (m, overlapped,8H), 3.01 (s, 12H), 3.00 (s, 12H).ESI-MS calcd for [M−PF_6]$^+$ (*m/z*): 1005.2525. Found: 1005.2532.

Synthesis of MOF-Ru1

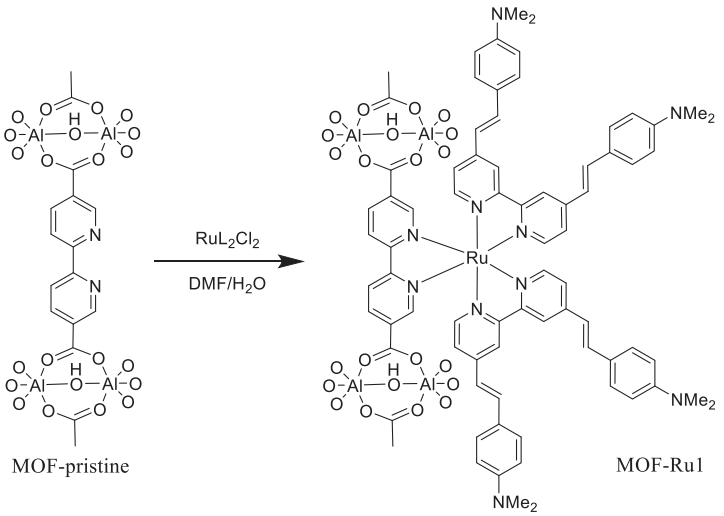

MOF-253(100 mg, 0.35 mmol) and [Ru((*E,E'*)-4,4′-Bis[*p*-(*N,N*-dimethylamino)styryl]-2,2′-bipyridine)$_2$Cl$_2$] (RuL_2Cl_2, 106 mg, 0.1 mmol) were stirred in DMF/H_2O (v/v, 30/30 mL) at 100°C under argon atmosphere for 8 h. After cooling down to room temperature, the dark-brown solid was obtained by filtration, and then washed with copious amount of DMF. The obtained product was further washed with methanol via soxhlet extraction for 24 h and dried in vacuum at 60°C. Yield: 59% (122 mg). ICP-MS analysis showed a Ru/Al molar ratio of 2.1%, indicating 2.1% of 2,2′-bipyridine-5,5′-dicarboxylic acid ligands in MOF-Ru1 were metalated with Ru.

Synthesis of MOF-Ru2

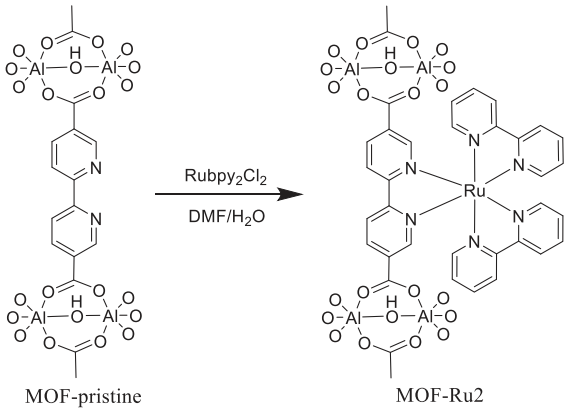

MOF-Ru2 was synthesized following a similar procedure for the synthesis of MOF-Ru1 using MOF-253(100 mg, 0.35 mmol) and Ru(2,2′-bipyridine)$_2$$Cl_2$ (48 mg, 0.1 mmol) as the starting materials. Yield: 43% (64 mg). ICP-MS analysis showed a Ru/Al molar ratio of 7.4%, indicating 7.4% of 2,2′-bipyridine-5,5′-dicarboxylic acid ligands in MOF-Ru2 were metalated with Ru.

Photocatalysis

General procedure for the photocatalytic C–N coupling reaction of benzylamine and its derivatives

A mixture of organic substrate (0.2 mmol) and MOF-Ru1 (10 mg) in CH_3CN (2 mL) was bubbled with O_2 for 2 min. The resulting solution was stirred at room temperature under 740 nm light irradiation for 5 h. After reaction, the mixture was centrifuged to remove MOF-Ru1. The supernatant liquid was then concentrated under reduced pressure to provide the desired product without further purification. The reaction yield was determined by ^{1}H NMR analysis using 3,4,5-trimethoxybenzaldehyde as an internal standard.

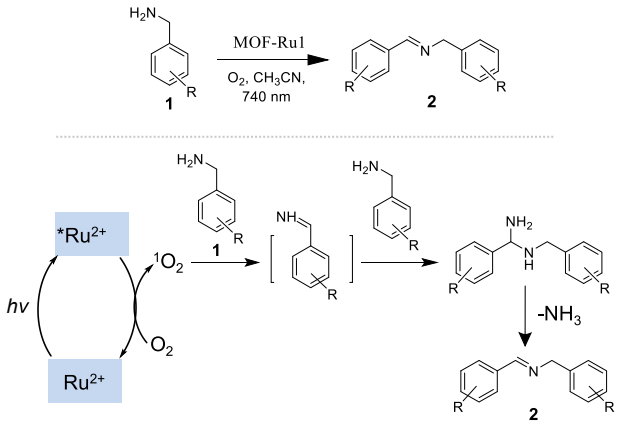

N-(Phenylmethylene)benzenemethanamine (2a)

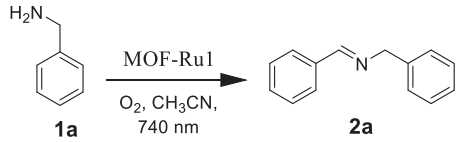

According to the general procedure, 1a (22 mg, 0.2 mmol) and MOF-Ru1 (10 mg) in CH_3CN (2 mL) afforded 2awith a yield of 93%.

^{1}H NMR ($CDCl_3$, 400 MHz): δ4.75 (s, 2H), 7.17 - 7.35 (m, overlapped, 8H), 7.70 (d, *J* = 8.9 Hz, 2H), 8.32 (s, 1H); ^{13}C NMR ($CDCl_3$, 125 MHz): δ162.0, 139.3, 136.1, 130.8, 128.6, 128.5, 128.3, 127.0, 65.1.

4-Fluoro-*N*-[(4-fluorophenyl)methylene]benzenemethanamine (2b)

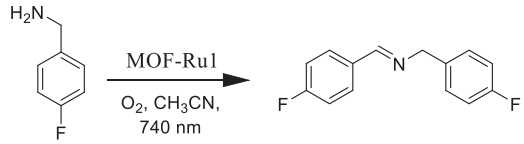

According to the general procedure, 1b (25 mg, 0.2 mmol) and MOF-Ru1 (10 mg) in CH_3CN (2 mL) afforded 2bwith a yield of 95%.

^{1} H NMR ($CDCl_3$, 400 MHz): δ4.69 (s, 2 H), 6.93 - 7.05 (m, overlapped, 4H), 7.18 - 7.24 (m, overlapped, 2H), 7.68 (dd, *J* = 5.6, 2.8 Hz, 2 H), 8.27 (s, 1 H); ^{13}C NMR ($CDCl_3$, 125 MHz): δ160.6, 130.2, 130.1, 129.5, 129.4, 115.9, 115.6, 115.4, 115.2, 64.2

4-Chloro-*N*-[(4-chlorophenyl)methylene]benzenemethanamine (2c)

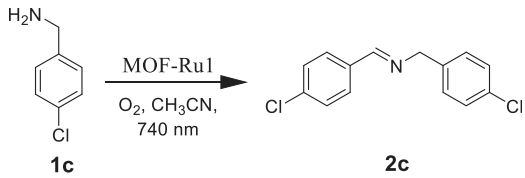

According to the general procedure, 1c (28 mg, 0.2 mmol) and MOF-Ru1 (10 mg) in CH_3CN (2 mL) afforded 2cwith a yield of 95%.

^{1}H NMR ($CDCl_3$, 400 MHz): δ4.70 (s, 2 H), 7.18 - 7.33 (m, overlapped, 6H), 7.63 (d, *J* = 8.4 Hz, 2 H), 8.27 (s, 1 H); ^{13}C NMR ($CDCl_3$, 125 MHz): δ160.9, 137.6, 136.9, 134.4, 132.8, 129.5, 129.3, 128.9, 128.6, 64.2

4-Bromo-*N*-[(4-bromophenyl)methylene]benzenemethanamine (2d)

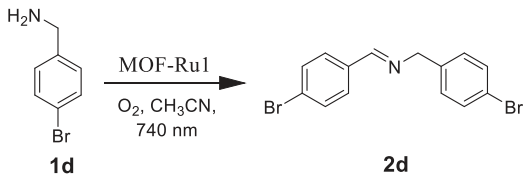

According to the general procedure, 1d (37 mg, 0.2 mmol) and MOF-Ru1 (10 mg) in CH_3CN (2 mL) afforded 2d with a yield of 98%.

^{1}H NMR ($CDCl_3$, 400 MHz): δ4.65 (s, 2 H), 7.11 (d, *J* = 8.0 Hz, 2 H), 7.37 (d, *J* = 8.6 Hz, 2 H), 7.45 (d, *J* = 8.4 Hz, 2 H), 7.54 (d, *J* = 8.5 Hz, 2 H), 8.24 (s, 1 H); ^{13}C NMR ($CDCl_3$, 125 MHz): δ161.0, 138.1, 134.8, 131.9, 131.6, 129.7, 125.4, 120.9, 64.2.

4-(Trifluoromethyl)-*N*-[[4-(trifluoromethyl)phenyl]methylene]benzenemethanamine (2e)

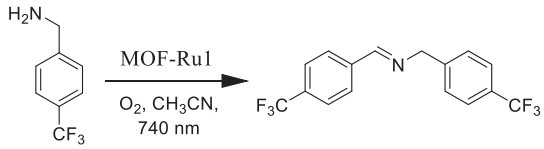

1e **2e**

According to the general procedure, 1e (35 mg, 0.2 mmol) and MOF-Ru1 (10 mg) in CH_3CN (2 mL) afforded 2e with a yield of 98%.

^{1}H NMR ($CDCl_3$, 400 MHz): δ4.90 (s, 2 H), 7.46 (d, *J* = 8.2 Hz, 2 H), 7.61 (d, *J* = 8.2 Hz, 2 H), 7.68 (d, *J* = 8.1 Hz, 2 H), 7.90 (d, *J* = 8.0 Hz, 2 H), 8.47 (s, 1 H); ^{13}C NMR ($CDCl_3$, 125 MHz): δ161.1, 142.9, 138.9, 132.7, 132.4, 128.5, 127.4 125.7, 125.6, 125.5, 64.2.

4-[[[(4-Cyanophenyl)methylene]amino]methyl]benzonitrile (2f)

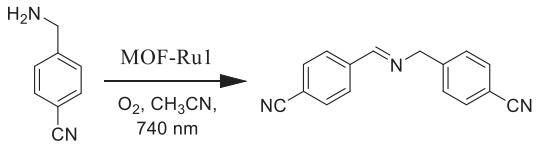

1f **2f**

According to the general procedure, 1f (27 mg, 0.2 mmol) and MOF-Ru1 (10 mg) in CH_3CN (2 mL) afforded 2f with a yield of 96%.

^{1}H NMR ($CDCl_3$, 400 MHz): δ3.72 (s, 3 H), 3.76 (s, 3 H), 3.65 (s, 3 H), 6.79 (dd, *J* = 8.9, 11 Hz, 4 H), 7.16 (d, *J* = 9.0 Hz, 2 H), 7.62 (d, *J* = 8.9 Hz, 2 H), 8.23 (s, 1 H); ^{13}C NMR ($CDCl_3$, 125 MHz): δ161.0, 144.2, 139.5, 132.5, 132.4, 128.7, 128.5, 118.9, 118.4, 114.4, 111.0, 64.3.

4-Methoxy-*N*-[(4-methoxyphenyl)methylene]benzenemethanamine (2 g)

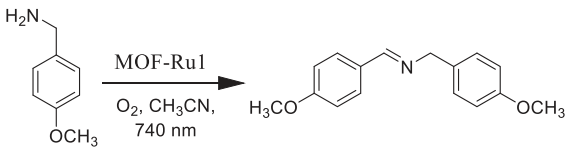

1g **2g**

According to the general procedure, 1 g (28 mg, 0.2 mmol) and MOF-Ru1 (10 mg) in CH_3CN (2 mL) afforded 2g in yield of 95%.

^{1}H NMR ($CDCl_3$, 400 MHz): δ3.72 (s, 3 H),3.76 (s, 3 H), 4.65 (s, 2 H), 6.79-6.86 (m, overlapped,4H), 7.16 (d, *J* = 9.0 Hz, 2 H), 7.62 (d, *J* = 6.6 Hz, 2 H), 8.22 (s, 1 H); ^{13}C NMR ($CDCl_3$, 125 MHz): δ161.7, 161.0, 158.6, 131.6, 129.8, 129.2, 129.1, 114.3, 114.0, 113.9, 64.4, 55.4, 55.3.

4-Methyl-*N*-[(4-methylphenyl)methylene]benzenemethanamine (2 h)

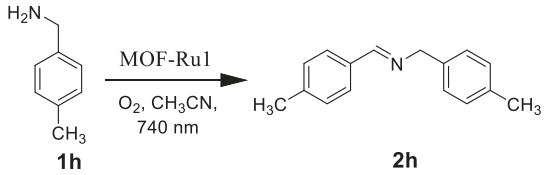

1h **2h**

According to the general procedure, 1 h (25 mg, 0.2 mmol) and MOF-Ru1 (10 mg) in CH_3CN (2 mL) afforded 2h with a yield of 93%.

^{1}H NMR ($CDCl_3$, 400 MHz): δ2.34 (s, 3 H), 2.39 (s, 3 H), 4.78 (s, 2 H), 7.14 - 7.24 (m, overlapped,6 H), 7.66 (d, *J* = 7.8 Hz, 2 H), 8.35 (s, 1 H); ^{13}C NMR ($CDCl_3$, 125 MHz): δ161.8, 141.0, 136.5, 136.3, 133.6, 129.3, 129.2, 128.3, 128.0, 64.8, 21.5, 21.1.

N-(2-Thienylmethylene)-2-thiophenemethanamine (2i)

1i **2i**

According to the general procedure, 1i (23 mg, 0.2 mmol) and MOF-Ru1 (10 mg) in CH_3CN (2 mL) afforded 2i with a yield of 91%.

^{1}H NMR ($CDCl_3$, 400 MHz): δ4.95 (s, 2 H), 6.97 - 7.00 (m, overlapped,2 H), 7.06 - 7.08 (m, overlapped,1 H), 7.23 - 7.26 (m, overlapped,1 H), 7.33 (d, *J* = 3.6 Hz, 1 H), 7.41 (d, *J* = 5.1 Hz, 1 H), 8.42 (s, 1 H); ^{13}C NMR ($CDCl_3$, 125 MHz): δ155.5, 142.1, 141.5, 131.0, 129.4, 127.4, 126.9, 125.4, 124.9, 58.5.

N-(1-Naphthalenylmethylene)-1-naphthalenemethanamine (2j)

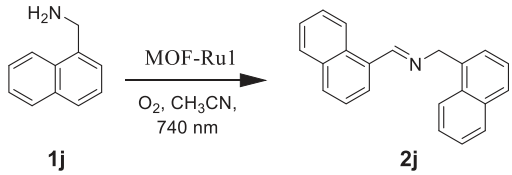

1j **2j**

According to the general procedure, 1j (32 mg, 0.2 mmol) and MOF-Ru1 (10 mg) in CH_3CN (2 mL) afforded 2j with a yield of 90%.

^{1}H NMR ($CDCl_3$, 400 MHz): δ5.42 (s, 2 H), 7.49 - 7.60 (m, overlapped,7 H), 7.83 - 7.97 (m, overlapped,5 H), 8.25 (d, *J* = 8.3 Hz, 1 H), 8.95 (d, *J* = 8.4 Hz, 1 H), 9.09 (s, 1 H); ^{13}C NMR ($CDCl_3$, 125 MHz): δ162.0, 135.5, 133.9, 133.8, 131.6, 131.3, 131.2, 129.2, 128.7, 127.8, 127.2, 126.2, 126.1, 125.9, 125.7, 125.3, 124.4, 124.0, 63.3.

Procedure for the relationship between the photocatalytic efficiency and photon power intensity

In order to obtain the relationship between the photocatalytic efficiency and photon power intensity, the photocatalytic C-N coupling reactions of benzyl amine were performed under 730 nm irradiation with different powers. A mixture of benzyl amine (50 mM) and MOF-Ru1 (10 mg) in CD_3CN (2 mL) was bubbled with O_2 for 2 min. The resulting solution was stirred at room temperature under 730 nm light irradiation with different powers (ranging from 68 mW to 476 mW) for 16 h. After reaction, the mixture was centrifuged to remove MOF-Ru1. The supernatant liquid was measured by ^{1}H NMR to obtain the yield.

General procedure for the photocatalytic hydrodebromination of α-bromoketones

A mixture of α-bromoketone (0.5 mmol), MOF-Ru1 (20 mg) and triethanolamine (TEOA, 5 mmol) in CH_3CN (10 mL) was bubbled with Ar for 15 min. The resulting suspension was stirred at room temperature under 740 nm light irradiation for 15 h. The solution was then filtrated. The obtained filtrate was concentrated under reduced pressure. The residue was purified by silica gel column chromatography (eluent: hexanes/ethyl acetate) to yield the desired product.

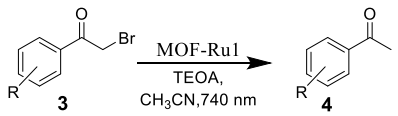

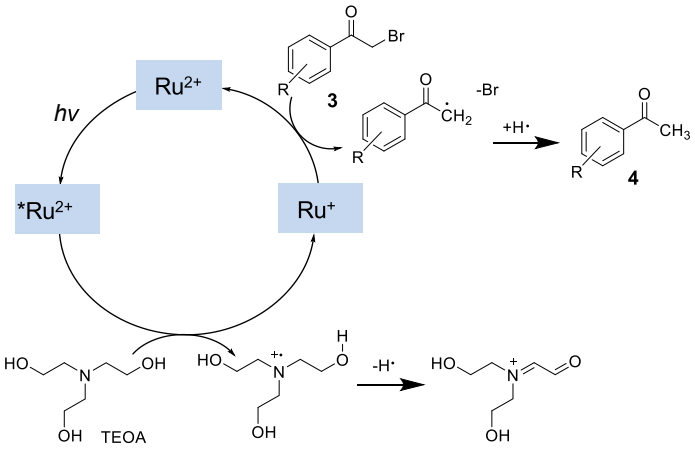

Acetophenone (4a)

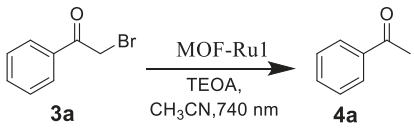

According to the general procedure, 3a (99 mg, 0.5 mmol), MOF-Ru1 (20 mg), and TEOA (746 mg, 5 mmol) in CH_3CN (10 mL) afforded 4a (51 mg, 85%) as a colorless oil after purification via silica gel column chromatography (hexanes/ethyl acetate, v/v = 100/3).

^{1}H NMR ($CDCl_3$, 400 MHz): δ2.60 (s, 3 H), 7.44 (t, *J* = 7.6 Hz, 2 H), 7.54 (t, *J* = 7.5 Hz, 1 H), 7.95 (d, *J* = 7.9 Hz, 2 H); ^{13}C NMR ($CDCl_3$, 125 MHz): δ198.2, 137.1, 133.1, 128.6, 128.3, 26.7.

4′-Methoxyacetophenone (4b)

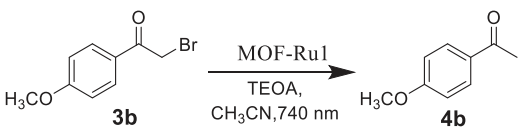

According to the general procedure, 3b (115 mg, 0.5 mmol), MOF-Ru1 (20 mg), and TEOA (746 mg, 5 mmol) in CH_3CN (10 mL) afforded 4b (65 mg, 87%) as a white solid after purification via silica gel column chromatography (hexanes/ethyl acetate, v/v = 100/3).

^1H NMR ($CDCl_3$, 400 MHz): δ2.55 (s, 3 H), 3.86 (s, 3 H), 6.92 (d, *J* = 8.8 Hz, 2 H), 7.92 (d, *J* = 8.8 Hz, 2 H); ^{13}C NMR ($CDCl_3$, 125 MHz): δ196.8, 163.5, 130.6, 130.3, 113.7, 55.5, 26.4.

4′-Fluoroacetophenone (4c)

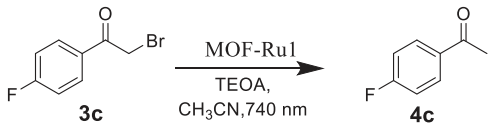

According to the general procedure, 3c (109 mg, 0.5 mmol), MOF-Ru1 (20 mg), and TEOA (746 mg, 5 mmol) in CH_3CN (10 mL) afforded 4c (55 mg, 80%) as a colorless oil after purification via silica gel column chromatography (hexanes/ethyl acetate, v/v = 100/3).

^1H NMR ($CDCl_3$, 400 MHz): δ2.59 (s, 3 H), 7.11 (t, *J* = 8.4 Hz, 2 H), 7.97 (dd, *J* = 5.5, 3.1 Hz, 2 H); ^{13}C NMR ($CDCl_3$, 125 MHz): δ196.5, 167.0, 164.5, 133.6, 131.0, 115.8, 115.6, 26.6.

4′-Chloroacetophenone (4d)

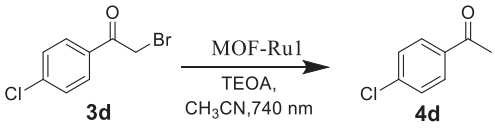

According to the general procedure,3d(117 mg, 0.5 mmol), MOF-Ru1(20 mg), and TEOA (746 mg, 5 mmol) in CH_3CN (10 mL) afforded 4d (63 mg, 82%) as a colorless oil after purification via silica gel column chromatography (hexanes/ethyl acetate, v/v = 100/3).

^1H NMR ($CDCl_3$, 400 MHz): δ2.58 (s, 3 H), 7.41 (d, *J* = 8.5 Hz, 2 H), 7.88 (d, *J* = 8.5 Hz, 2 H); ^{13}C NMR ($CDCl_3$, 125 MHz): δ196.8, 139.6, 135.4, 129.7, 128.9, 26.6.

4′-Bromoacetophenone (4e)

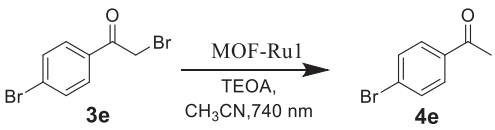

According to the general procedure, 3e (140 mg, 0.5 mmol), MOF-Ru1 (20 mg), and TEOA (746 mg, 5 mmol) in CH_3CN (10 mL) afforded 4e (86 mg, 87%) as a white solid after purification via silica gel column chromatography (hexanes/ethyl acetate, v/v = 100/3).

^1H NMR ($CDCl_3$, 400 MHz): δ2.57 (s, 3 H), 7.57 (d, *J* = 8.5 Hz, 2 H), 7.79 (d, *J* = 8.5 Hz, 2 H); ^{13}C NMR ($CDCl_3$, 125 MHz): δ197.0, 135.8, 131.9, 129.8, 128.3, 26.6.

4-Acetylbenzonitrile (4f)

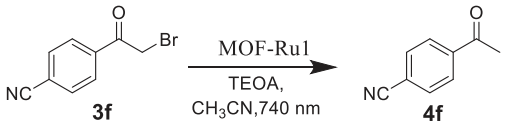

According to the general procedure, 3f (112 mg, 0.5 mmol), MOF-Ru1 (20 mg), and TEOA (746 mg, 5 mmol) in CH_3CN (10 mL) afforded 4f (60 mg, 82%) as a white solid after purification via silica gel column chromatography (hexanes/ethyl acetate, v/v = 100/10).

^{1}H NMR ($CDCl_3$, 400 MHz): δ2.68 (s, 3 H), 8.10 (d, *J* = 6.9 Hz, 2 H), 8.30 (d, *J* = 6.7 Hz, 2 H); ^{13}C NMR ($CDCl_3$, 125 MHz): δ196.3, 150.4, 141.4, 129.3, 123.9, 27.0.

4′-Nitroacetophenone (4g)

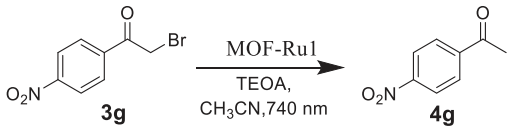

According to the general procedure,3g(122 mg, 0.5 mmol), MOF-Ru1(20 mg), and TEOA (746 mg, 5 mmol) in CH_3CN (10 mL) afforded 4g (70 mg, 84%) a white solid after purification via silica gel column chromatography (hexanes/ethyl acetate, v/v = 100/3).

^{1}H NMR ($CDCl_3$, 400 MHz): δ2.62 (s, 3 H), 8.04 (d, *J* = 8.9 Hz, 2 H), 8.24 (d, *J* = 8.9 Hz, 2 H); ^{13}C NMR ($CDCl_3$, 125 MHz): δ196.4, 150.3, 141.1, 129.3, 123.9, 27.0.

2-Acetonaphthone (4h)

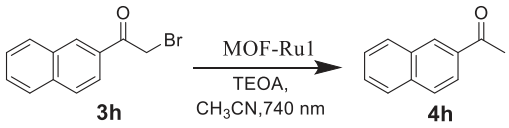

According to the general procedure,3h(125 mg, 0.5 mmol), MOF-Ru1(20 mg), and TEOA (746 mg, 5 mmol) in CH_3CN (10 mL) afforded 4h (76 mg, 89%) as a white solid after purification via silica gel column chromatography (hexanes/ethyl acetate, v/v = 100/5).

^{1}H NMR ($CDCl_3$, 400 MHz): δ2.73 (s, 3 H), 7.53 - 7.62 (m, 2 H), 7.86 - 7.90 (m, 2 H), 7.95 (d, *J* = 8.1 Hz, 1 H), 8.02 (dd, *J* = 1.8, 6.8 Hz, 1 H), 8.46 (s, 1 H); ^{13}C NMR ($CDCl_3$, 125 MHz): δ198.1, 135.6, 134.5, 132.5, 130.2, 129.6, 128.5, 128.4, 127.8, 126.8, 123.9, 26.7.

General procedure for the photocatalytic hydroxylation of arylboronic acids

A solution of arylboronic acid (0.2 mmol), MOF-Ru1 (10 mg), *N,N*-diisopropylethylamine (^{i}Pr$_2$NEt,0.4 mmol) in DMF (2.0 mL) was bubbled with O_2 for 1 min. The resulting reaction mixture was stirred at room temperature under 740 nm light irradiation for 5 h. The suspension was then centrifuged at 6000 rpm to remove the solid component. The obtained solution was added into 30 mL H_2O and

then extracted with ethyl acetate (3 ×30 mL). The combined organic solution was washed with brine, dried with Na_2SO_4, and concentrated under reduced pressure to provide the desired product without further purification. The reaction yield was determined by ^{1}H NMR analysis using 3,4,5-trimethoxybenzaldehyde as an internal standard.

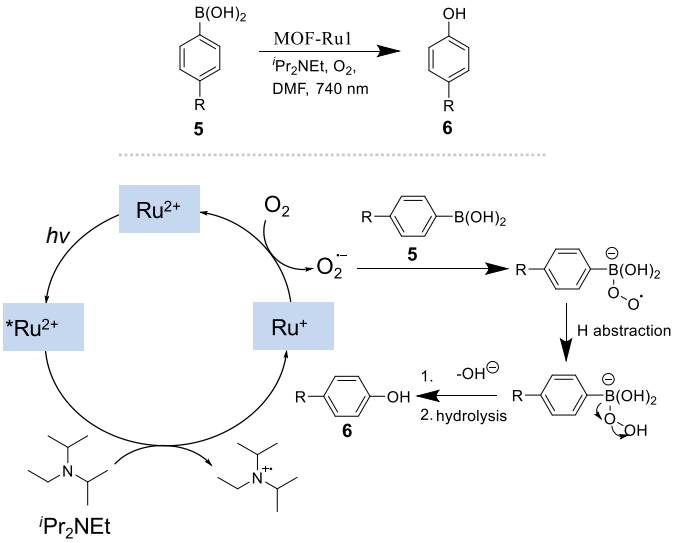

Phenol (6a)

According to the general procedure, 5a (25 mg, 0.2 mmol), MOF-Ru1 (10 mg), and ^{i}Pr$_2$NEt (52 mg, 0.4 mmol) in DMF (2 mL) afforded 6a as a colorless oil with a yield of 90%.

^{1}H NMR ($CDCl_3$, 400 MHz): δ4.97 (s, 1 H), 6.78 (d, J = 8.6 Hz, 2 H), 6.84 (t, J = 7.4 Hz, 1 H), 7.15 (t, J = 8.0 Hz, 2 H); ^{13}C NMR ($CDCl_3$, 125 MHz): δ155.4, 129.7, 120.8, 115.3.

4-Methoxyphenol (6b)

According to the general procedure, 5b (30 mg, 0.2 mmol), MOF-Ru1 (10 mg), and ^{i}Pr$_2$NEt (52 mg, 0.4 mmol) in DMF (2 mL) afforded 6b as a colorless oil with a yield of 88%.

^{1}H NMR ($CDCl_3$, 400 MHz): δ 3.76 (s, 3 H), 6.75 (d, 4 H); ^{13}C NMR ($CDCl_3$, 125 MHz): δ153.6, 149.7, 116.1, 114.8, 55.8.

4-Chlorophenol (6c)

According to the general procedure, 5c (31 mg, 0.2 mmol), MOF-Ru1 (10 mg), and $^{i}Pr_2NEt$ (52 mg, 0.4 mmol) in DMF (2 mL) afforded 6c as a pale yellow solid with a yield of 92%.

^{1}H NMR ($CDCl_3$, 400 MHz): δ6.77 (d, *J* = 7.9 Hz, 2 H), 7.17 (d, *J* = 7.8 Hz, 2 H); ^{13}C NMR ($CDCl_3$, 125 MHz): δ154.4, 129.5, 125.4, 116.7.

p-Hydroxybenzaldehyde (6d)

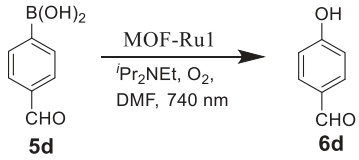

According to the general procedure, 5d (30 mg, 0.2 mmol), MOF-Ru1 (10 mg), and $^{i}Pr_2NEt$ (52 mg, 0.4 mmol) in DMF (2 mL) afforded 6d as a light yellow solid with a yield of 76%.

^{1}H NMR ($CDCl_3$, 400 MHz): δ 6.97 (d, *J* = 8.0 Hz, 2 H), 7.79 (d, *J* = 7.9 Hz, 2 H), 9.84 (s, 1 H); ^{13}C NMR ($CDCl_3$, 125 MHz): δ191.3, 162.1, 132.5, 129.6, 116.1.

4-Phenylphenol (6e)

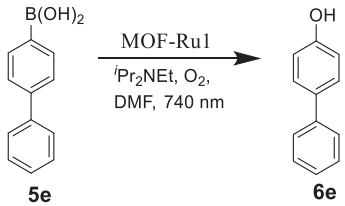

According to the general procedure, 5e (40 mg, 0.2 mmol), MOF-Ru1 (10 mg), and $^{i}Pr_2NEt$ (52 mg, 0.4 mmol) in DMF (2 mL) afforded 6e as a light yellow solid with a yield of 90%.

^{1}H NMR ($CDCl_3$, 400 MHz): δ 6.91 (d, *J* = 8.2 Hz, 2 H), 7.29 (t, *J* = 7.6 Hz, 1 H), 7.40 (t, *J* = 7.4 Hz, 2 H), 7.48 (d, *J* = 8.1 Hz, 2 H), 7.54 (d, *J* = 8.0 Hz, 2 H); ^{13}C NMR ($CDCl_3$, 125 MHz): δ155.2, 140.8, 133.9, 128.7, 128.4, 126.7, 115.7.

Redox neutral photoredox catalysis -C-H cyanation of tetrahydroisoquinoline

Starting material preparation

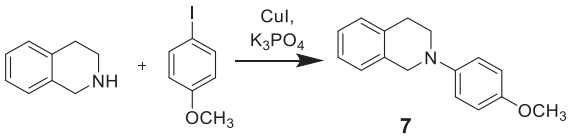

A mixture of 1,2,3,4-tetrahydroisoquinoline (0.63 mL, 5 mmol) and 4-iodoanisole (1.2 g, 5 mmol), copper(I) iodide (95.3 mg, 0.5 mmol) and potassium phosphate (2.1 g, 10 mmol) in 2-propanol/ethylene glycol (20/2, v/v) was refluxed at 80°C for 24 h under argon atmosphere. After cooling down to room temperature, the mixture was quenched by water (50 mL) and extracted with ethyl acetate (30mL× 3). The organic layer was concentrated under reduced pressure via rotary evaporation. The obtained residue was purified by silica gel column chromatography to afford the white solid product (860 mg, 72%).

^{1}H NMR ($CDCl_3$, 400 MHz): δ 3.04 (t, *J* = 5.7 Hz, 2 H), 3.50 (t, *J* = 5.8 Hz, 2 H), 3.84 (s, 3H), 4.37 (s, 2H), 6.96 (d, *J* = 9.0 Hz, 2 H), 7.05 (d, *J* = 9.0 Hz, 2 H), 7.19 - 7.25 (m, overlapped, 4H); ^{13}C NMR ($CDCl_3$, 125 MHz): δ153.5, 145.4, 134.7, 134.6, 128.8, 126.6, 126.3, 126.0, 118.1, 114.6, 55.7, 52.7, 48.5, 29.2.

General procedure

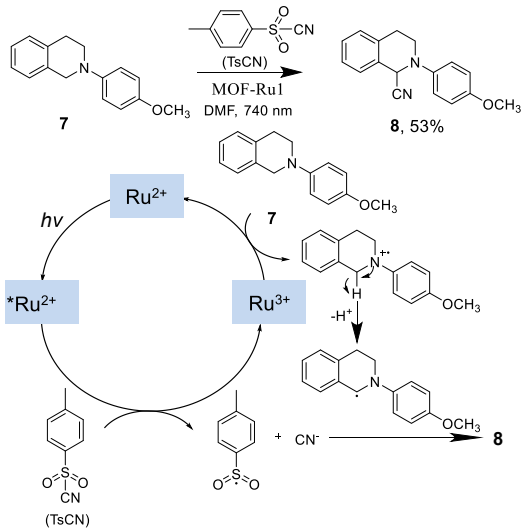

A solution of 7 (48 mg, 0.2 mmol), *p*-toluene sulfonyl cyanide (TsCN, 36 mg, 0.2 mmol), MOF-Ru1 (10 mg) in DMF (2 mL) was bubbled with Ar for 15 min. The resulting suspension was stirred at room temperature under 740 nm light irradiation for 5 h. The suspension was then centrifuged at 6000 rpm to remove the solid component. The liquid solution was concentrated under reduced pressure. The obtained residue was purified by silica gel column chromatography to afford the colorless oil product 8 (27 mg, 53%).

^{1}H NMR ($CDCl_3$, 400 MHz): δ 2.84 - 2.89 (m, overlapped, 1H), 3.06 - 3.14 (m, overlapped, 1H), 3.33 - 3.40 (m, overlapped, 1H), 3.49 - 3.54 (m, overlapped, 1H), 3.73 (s, 3H), 5.30 (s, 1H), 6.84 (d, *J* = 10.7 Hz, 2 H), 7.01 (d, *J* = 10.6 Hz, 2 H), 7.15 - 7.25 (m, overlapped, 4H); ^{13}C NMR ($CDCl_3$, 125 MHz): δ155.7, 142.6, 134.4, 129.7, 129.5, 128.7, 127.1, 126.7, 121.0, 117.6, 114.8, 55.7, 55.6, 44.9, 28.7.

General procedure for the photocatalytic atom transfer radical polymerization of methyl methacrylate

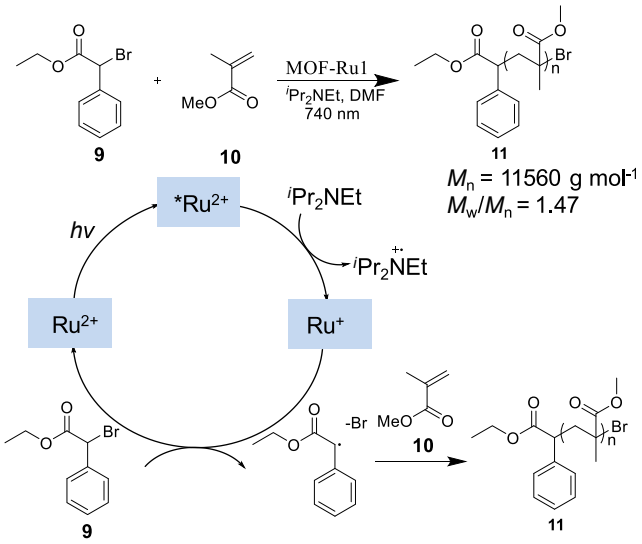

A mixture of 9 (88 μL, 0.5 mmol), 10 (266 μL, 2.5 mmol) and MOF-Ru1 (10 mg) in DMF (1 mL) was degassed by freeze-pump-thaw cycles for 4 times. The mixture was stirred at room temperature under 740 nm light irradiation for 15 h under at 22°C. After reaction, the suspension was then centrifuged at 14000 rpm to remove the solid component. The liquid solution was added to a cold mixture of methanol/water (v/v = 10/1, 30 mL) solution. The white precipitate was filtered and dried to give the desired product. M_n = 11560 gmol^{-1}, M_w/M_n = 1.47.